Dynamics of Optomechanical Droplets in a Bose-Einstein Condensate

J.G.M. Walker,* G.R.M. Robb, G.-L. Oppo, and T. Ackemann
SUPA and Department of Physics, University of Strathclyde, Glasgow G4 0NG, Scotland, United Kingdom

(Dated: May 21, 2022)

We investigate numerically a one-dimensional Bose-Einstein Condensate illuminated by off-resonant laser light which is retroreflected by a single feedback mirror. Studying the ground states of the system, we find density structures which are self-trapped via the optomechanical action of the diffracted light. We show that these structures are stable and exhibit Newtonian dynamics. We propose that these results allow continuous, non-destructive monitoring of condensate dynamics via the optical intensity and may offer new opportunities for optical control and transport of coherent matter via gradients in optical phase alone.

I. INTRODUCTION

Self-organized patterns and structures that arise due to a combination of optical nonlinearity and diffraction have been predicted and observed in a variety of media [1–10] including specifically atomic vapours [1–6, 11–13]. In recent times, there has been significant interest in self-organisation phenomena involving cold and ultracold atomic gases e.g. cold atoms or a Bose-Einstein Condensate (BECs) interacting with one or more modes of an optical cavity [14–19], which have resulted in a wide range of new nonlinear and quantum phenomena e.g. collective atomic recoil lasing (CARL) [14, 20], Dicke superradiance [21] and supersolid formation [22–24]. In these systems, the source of optical nonlinearity is optomechanical i.e. the centre-of-mass motion of the atoms under the mechanical action of light, specifically optical dipole forces. Optomechanical self-structuring of a cold thermal gas has been studied experimentally and theoretically in systems of counterpropagating beams in [25, 26] and, as is modelled here, in a single mirror feedback (SMF) configuration in [27, 28], with diffraction of light providing spatial coupling between different parts of the BEC. The concept of optomechanical self-structuring was extended theoretically from the case of a thermal gas to a BEC in [29]. It was shown that a significant difference with the behaviour in a classical, thermal gas, was due to the presence of "quantum pressure" i.e. the dispersive nature of the BEC wavefunction, which acts to damp out density modulations or spatial structure in the BEC. Recent work has shown that in addition to global patterns, the system can display a spatially localised structures termed "droplets" or "quantum droplets" both in the SMF configuration [30, 31] and in a ring-cavity setup [32]. These droplets are self-bound optomechanical structures consisting of interacting light and matter. They display some similar characteristics to quantum droplets in other systems e.g. dipolar BECs [33] but are also similar in some respects to other types of spatially-localised structures e.g. spatial solitons [34]. In this paper we study the dynamical behaviour of these optomechanical droplets in 1D in a configuration involving a single feedback mirror, as in [30, 31].

II. MODEL

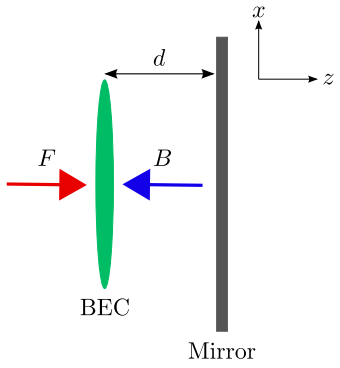

FIG. 1. Schematic diagram of the single mirror feedback (SMF) configuration.

Here we model the optomechanical behaviour of a BEC present within a SMF configuration as is shown diagramatically in Fig. 1. We take a similar approach to [29] to model the dilute, non-interacting BEC where we use a Schrodinger equation which describes the evolution of the BEC wavefunction, $\Psi(x,t)$, as:

$$i\hbar\frac{\partial\Psi(x,t)}{\partial t} = -\frac{\hbar^2}{2m}\frac{\partial^2\Psi(x,t)}{\partial x^2} + V(x,t)\Psi(x,t) \qquad (1)$$

where we consider a potential energy, V, to be given by:

$$V(x,t) = \frac{\hbar\delta}{2}\left(|F|^2 + |B(x,t)|^2\right), \qquad (2)$$

and where m is the atomic mass, $\delta = \omega - \omega_a$ where ω and ω_a are the optical field frequency and atomic transition resonance frequency respectively, $s = |F|^2 + |B(x,t)|^2$

* josh.walker@strath.ac.uk

This is a peer reviewed, accepted author manuscript of the following research article: Walker, J., Robb, G., Oppo, G-L., & Ackemann, T. (2022). Dynamics of optomechanical droplets in a Bose-Einstein condensate. Physical Review A, 105, [063305]. https://doi.org/10.1103/PhysRevA.105.063305

is the saturation parameter due to the forward and backwards fields, which are given by $|F,B|^2 = \frac{I_{F,B}}{I_{\rm sat}\Delta^2}$ with $I_{F,B}$ the intensity of the forward (F) or backward (B) beam, $I_{\rm sat}$ is the saturation intensity on resonance, $\Delta = \frac{2\delta}{\Gamma}$ and Γ is the decay rate of the atomic transition. It has been assumed that $|\Delta| \gg 1$ and that consequently $s \ll 1$ so that the atoms remain in their ground state. In addition, longitudinal grating effects due to interference between the counter-propagating optical fields on the transverse pattern formation process are neglected.

In order to describe the optical field evolution we assume that the gas is sufficiently thin that diffraction can be neglected, so that the forward field transmitted through the cloud is

$$F_{tr} = \sqrt{p_0}\exp\left(-i\chi_0 n(x,t)\right) \tag{3}$$

where $p_0 = |F(z=0)|^2$ is the scaled pump intensity incident on the atoms, $\chi_0 = \frac{b_0}{2\Delta}$ is the susceptibility of the cloud, b_0 is the optical thickness of the cloud at resonance and $n(x,t) = |\Psi(x,t)|^2$ is the local density of the BEC. We consider that the total density is conserved and as such the assumption of a preserved number of atoms is made.

To complete the feedback loop, calculation of the backward field, B at the atomic cloud is required. As the field propagates a distance $2d$ from the cloud to the mirror and back, optical diffraction plays a crucial role by converting phase modulations to amplitude modulations and consequently optical dipole forces. The relation between the Fourier components of the forward and backward fields at the cloud is

$$B(q) = \sqrt{R}F_{tr}(q)e^{-i\frac{q^2 d}{k_0}} \tag{4}$$

where R is the mirror reflectivity, q is the transverse wavenumber, $k_0 = \frac{2\pi}{\lambda_0}$ and it has been assumed $q \ll k_0$. It has also been assumed that the propagation time of the light between the BEC and mirror is sufficiently small as to be neglected.

Eq. (1), (3) and (4) can be solved self-consistently to describe the mutual interaction of the moving atoms and the optical fields. Numerical integration of these equations is performed to obtain the spatiotemporal dynamics of the BEC within the SMF setup. Transformation to imaginary time ,$\tau = -it$, is also performed here and the same equations numerically intergrated with an inital Gaussian density distribution to obtain the ground state solutions.

III. OPTOMECHANICAL PATTERNS AND DROPLETS

A. Optomechanical Patterns

The existence of optomechanical patterns in a dilute BEC illuminated by an optical field retro-reflected by a SFM was first predicted in [29] using a 1D model. These patterns form as a result of a self-structuring instability in which a spatially homogeneous optical field and BEC density become unstable, resulting in the spontaneous formation of periodic modulations in both the optical intensity and BEC density. The physical origin of the instability is the Talbot effect, which converts phase modulation in the optical field produced by BEC density fluctuations to intensity modulations and consequently optical dipole forces which increase density modulation. An example of this pattern formation is shown in Fig. 2. The system develops a modulated optical intensity and modulated BEC density with a spatial period of $\Lambda_c = \frac{2\pi}{q_c}$, where

$$q_c = \sqrt{\frac{\pi}{2}\frac{k_0}{d}}. \tag{5}$$

From q_c we define $\omega_r = \frac{\hbar q_c^2}{2m}$, analogous to the recoil frequency associated with momentum changes of $\hbar q_c$.

The reason for this instability is that BEC density modulations (which correspond to refractive index modulations of the BEC) with spatial frequency q_c, produce phase modulations in F_{tr} which are in turn converted into intensity modulations of B (see Eq.(4)) [35]. These intensity modulations produce dipole forces, which in turn reinforce density modulations, resulting in positive feedback and instability of the initial, homogeneous state. More recently, 2D patterns and droplet formation in a SFM configuration was studied in [30, 31], including the effects of direct atom-atom interactions via the BEC scattering length.

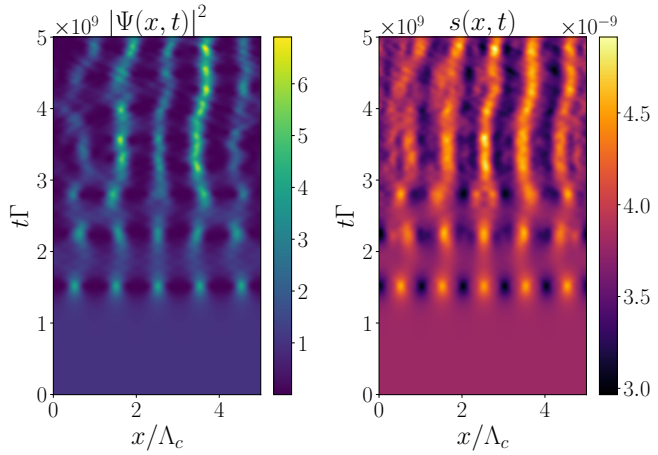

FIG. 2. Example of pattern formation/self-structuring of a BEC in a single feedback mirror configuration. Parameters used here are: $p_0 = 1.9\times10^{-9}$, $\Delta = -100$, $R = 0.99$, $\omega_r/\Gamma = 9.88\times10^{-9}$ and $b_0 = 20$.

B. Optomechanical Droplets

1. *Stable droplets*

In section III A, the initial conditions correspond to a spatially homogeneous optical intensity and BEC density which exhibits a self-structuring instability and evolves into a quasi-stationary state which consists of a strongly modulated pattern with some temporal variation in the amplitude of the pattern maxima and minima. However, simulations involving imaginary time propagation demonstrate that the ground states of this system are localised structures of BEC density and corresponding optical intensity, as originally predicted in [30] where a nonlinearity due to a combination of optomechanical forces and atomic collisions was investigated. Here we concentrate on a regime in which effects due to atomic collisions (or atomic scattering length) are negligible and structures are produced due to optomechanical forces alone. The temporal evolution of these stable optomechanical droplets is shown in Figs. 3 and 4 for both red-detuning ($\Delta < 0$) and blue-detuning ($\Delta > 0$) respectively. It can be seen that for red-detuning, the maxima of the BEC density and optical intensity coincide due to the potential energy of the system being minimised when atoms sit at positions of maximum optical intensity. In contrast, for blue-detuning the maximum of the BEC density coincides with a minimum of optical intensity. The properties of the stable ground state droplet are determined in full by the optical parameters of the system such as detuning, pump intensity and mirror-distance, d (via q_c).

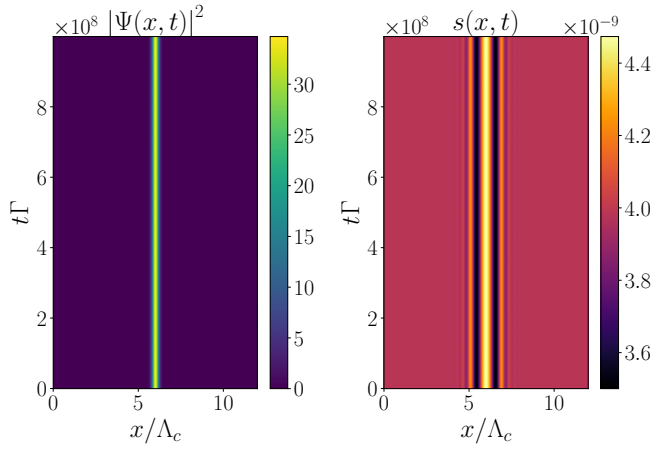

FIG. 3. Evolution of a stable optomechanical droplet for red-detuning. Parameters used are: $p_0 = 2.0 \times 10^{-9}$, $\Delta = -800$, $R = 0.99$, $\omega_r/\Gamma = 5.69 \times 10^{-8}$ and $b_0 = 20$.

To observe a fully static droplet in time-dependent simulations using Eq. (1), (3) and (4) requires the BEC density profile to exactly match the ground state profile. However, the system continues to support droplet

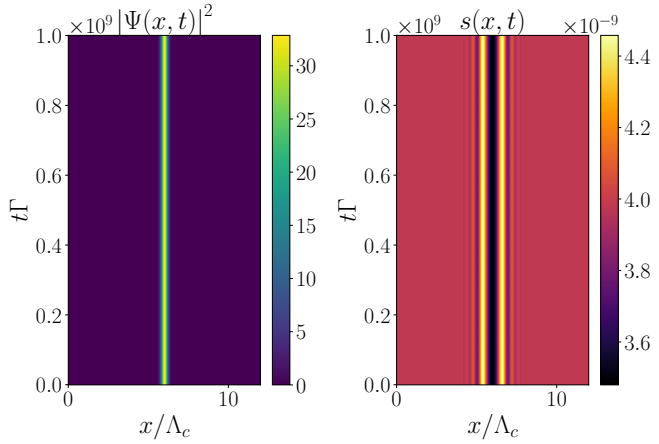

FIG. 4. Evolution of a stable optomechanical droplet for blue-detuning. Parameters used are: $p_0 = 2.0 \times 10^{-9}$, $\Delta = 800$, $R = 0.99$, $\omega_r/\Gamma = 5.69 \times 10^{-8}$ and $b_0 = 20$.

structures with an initial BEC density profile which is perturbed from the ground state. With such initial conditions the system exhibits now dynamical behaviour, with density oscillations as the self-imposed trapping potential from the optical intensity continually adjusts to the changing BEC density profile. This behaviour is shown in Fig. 5.

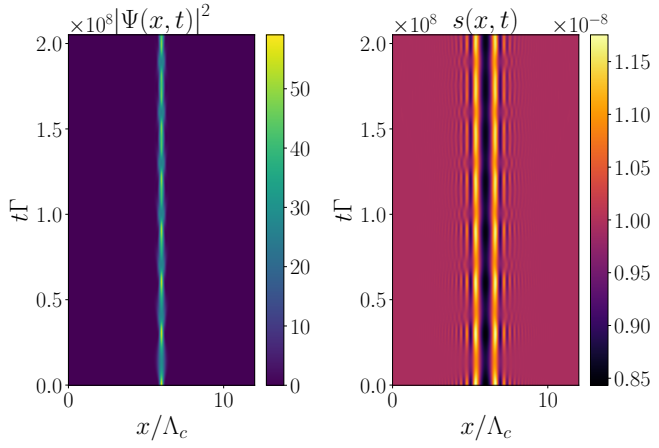

FIG. 5. Evolution of a perturbed blue-detuned droplet, where the initial BEC density has been produced from a Gaussian distribution whose width is adjusted slightly from the ideal value. Parameters used are: $p_0 = 5.0 \times 10^{-9}$, $\Delta = 800$, $R = 0.99$, $\omega_r/\Gamma = 5.69 \times 10^{-8}$ and $b_0 = 20$.

For both the self-structuring patterned state and perturbed droplet profiles we can observe temporal variation consistent with a system which is a superposition of eigenstates rather than in the ground state. In this conservative system the patterned state is a asymptotic state, however with the inclusion of damping and friction,

the system would be expected to relax to the droplet state as it is a ground state of the system, as demonstrated by the imaginary time simulations.

Quantum pressure in the BEC plays an important role in stabilising the droplet against compression, and is capable of producing a stable droplet even in the absence of other dispersive effects such as finite temperature or repulsive collisions (positive scattering length). It can be shown that the presence of quantum pressure is required to produce a minimised ground state energy with non-zero droplet width [36, 37]. For narrow droplets an additional stabilising factor is diffraction, which will produce a lower limit to the width of the optical potential associated with the droplet.

2. *Single and multiple peak droplet structures*

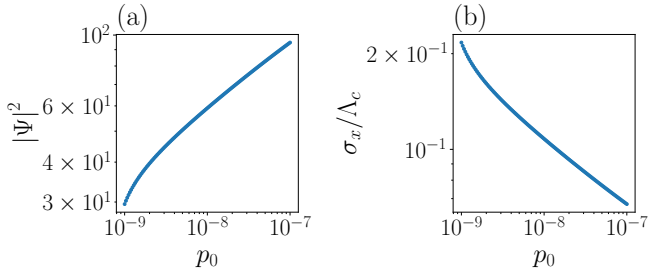

FIG. 6. Droplet width, σ_x, and peak density $|\Psi|^2$ against pump intensity, p_0, shown in panels (a) and (b) respectively. Results were calculated through imaginary time integration with parameters; $R = 0.99$, $\omega_r/\Gamma = 1.01 \times 10^{-7}$, $\Delta = 800$ and $b_0 = 20$.

Fig. 6 shows the dependence of the width and amplitude of the BEC density on pump intensity, p_0, when a stable droplet forms. It can be seen that as the pump intensity is increased, the droplet narrows and the peak of the BEC density increases. It can also be seen that the width of the droplet has a power-law dependence on p_0, scaling as $\sigma_x \propto {p_0}^{-1/4}$, in agreement with analytical predictions of the droplet width in the limit where $\chi|\Psi|^2 \ll 1$ [36, 37].

When the pump is red-detuned ($\Delta < 0$), then in addition to the single-peaked droplet structures shown previously, structures consisting of multiple density peaks also arise. Examples of these multi-peak droplet structures are shown in Fig. 7 (b) & (c) which show double and triple peaked droplet structures respectively. Complex, multiple droplet structures were observed in [30, 31] but their physical origin is different as their existence was reported only for non-zero BEC scattering length, whereas

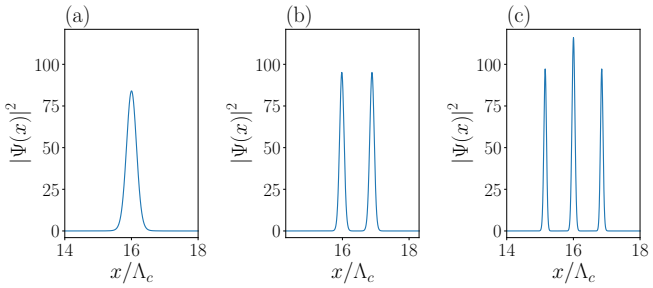

FIG. 7. Example ground state droplet density profiles for red detuning, calculated from imaginary time integration. Panels (a), (b) and (c) show the density profiles of single, dual and triple peak droplet structures respectively. Parameters used are; $R = 0.99$, $\omega_r/\Gamma = 4.05 \times 10^{-7}$, $b_0 = 20$ and $\Delta = -800$ with pump intensity, p_0, for (a), (b) and (c) being 3.714×10^{-9}, 2.395×10^{-8} and 9.398×10^{-8} respectively. Panel (b) shows an off centre structural position, consistent with the translational invariance of the system.

here we exclusively consider the case for no internal interactions.

These multiple droplet structures have not been observed in numerical simulations for cases involving blue-detuning ($\Delta > 0$). The reason for the different behaviour of the system when red and blue detuned is due to the combined effect of refraction in the narrow BEC and diffraction between the BEC and mirror, which produces the corresponding optical intensity profile and consequent (dipole) potential energy profile. The BEC acts like a narrow refractive element, which affects the optical phase as described by Eq. 3. Its refractive effect is dependent on χ_0 and consequently on Δ. The resulting diffraction pattern after propagation of the transmitted optical field from the BEC to the mirror and back will also therefore depend on Δ. The most significant difference is in relative amplitudes of the off-axis maxima and minima of the diffraction pattern. As shown in Fig. 3(b) and 4(b), for ($\Delta > 0$) the pattern consists of a central minimum, with a series of damped oscillations off-centre which are characteristic of Fresnel diffraction. For ($\Delta < 0$) the pattern consists of a central maximum, with damped oscillations off-centre. As pump intensity p_0 is increased, the width of the BEC decreases as shown in Fig. 6, which causes the amplitude of the off-centre diffractive minima/maxima to increase relative to the central one [35].

In the case of red-detuning these off-centre maxima grow to become the global maxima of the optical intensity profile. This results in an energetically favourable configuration when the BEC occupies the off-centre locations of peak optical intensity instead of occupying the central local maximum. Fig. 8(a) shows the case for a global central peak where a single peak droplet is the ground state configuration. Fig. 8(b) shows that, for an increased pump amplitude relative to Fig. 8(a), the off-centre maxima are now the global maxima. As pump amplitude is increased further a transition to the two

peak droplet ground state is observed at which point the optical intensity profile takes the form shown in Fig. 8(c). For blue detuning the off-centre minima do not grow to become global minima of the intensity profile for any of the parameters examined here.

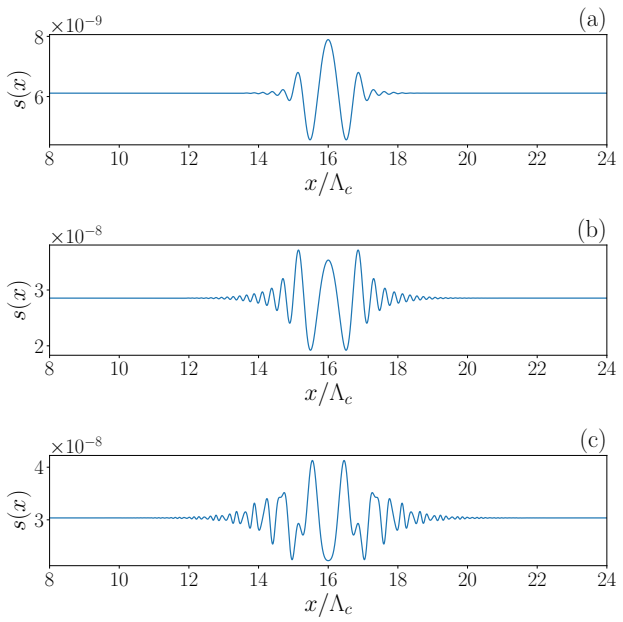

FIG. 8. Ground state optical field intensity profiles for red detuned system with pump amplitudes $p_0 = 3.07 \times 10^{-9}$, $p_0 = 1.43 \times 10^{-8}$ and $p_0 = 1.53 \times 10^{-8}$ for (a), (b) and (c) respectively. Calculated from imaginary time integration. Additional parameters used are; $R = 0.99$, $\omega_r/\Gamma = 4.05 \times 10^{-7}$, $\Delta = -800$ and $b_0 = 20$.

3. *Dynamic droplets*

It has been established that the BEC and optical fields can form a stationary, stable droplet. We now consider the dynamics of moving droplets, with first the addition of a uniform velocity. Providing our initial BEC wavefunction with an additional linear phase gradient will imprint this initial velocity on the droplet.

$$\Psi(x, t = 0) = \sqrt{n_0(x)}\, e^{imv_0 x/\hbar} \tag{6}$$

Such a phase gradient is given in Eq. 6, where $n_0(x)$ is the initial density profile of the BEC (the ground state droplet profile), v_0 is the uniform BEC velocity and m is the mass of each atom in the BEC.

Figs. 9 and 10 show the evolution of the BEC and optical fields for both red and blue detuning respectively. These droplets continue to be stable like their static counterparts, which were shown in Figs. 3 and 4. In both cases the optical field distribution also moves with uniform velocity, tracking the uniformly moving BEC. In the case of red detuning, Fig. 9, this results in an optical intensity maximum which always coincides with the BEC, whereas in the case of blue detuning, Fig. 10, an optical intensity minimum always coincides with the BEC.

Dynamics of similar self-trapping BEC structures have been studied for a ring-cavity configuration [32] where a friction like force was found to damp out motion of the density structures. This friction arises in the ring-cavity case from the finite response time of the cavity which allows optical intensity profiles to lag behind changes in BEC density. Although mirror loss is included within our model the finite time for propagation of light through the system is neglected resulting in the undamped motion seen here.

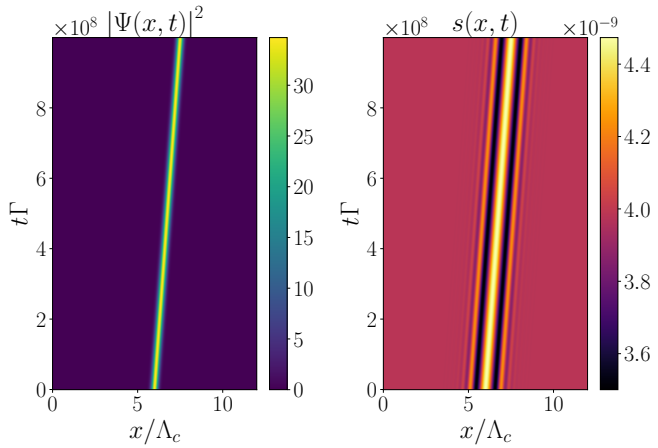

FIG. 9. Uniformly moving droplet for red-detuning ($\Delta < 0$). Parameters used are identical to those of Fig. 3 with the addition of $v_0 = \hbar q_c/12m$.

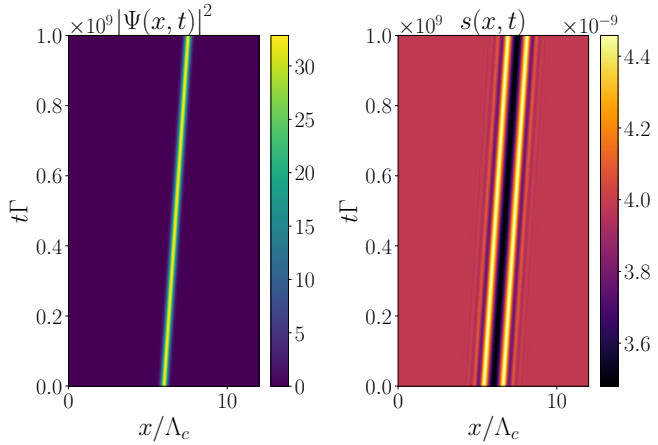

FIG. 10. Uniformly moving droplet for blue-detuning ($\Delta > 0$). Parameters used are identical those of Fig. 4 with the addition of $v_0 = \hbar q_c/12m$.

Similarly, we can investigate the stability and behaviour of these droplets under uniform acceleration. An acceleration can be achieved with the modification of the potential energy given in Eq. 7 where a is the constant acceleration.

$$V(x,t) = \frac{\hbar\delta}{2}\left(|F|^2 + |B(x,t)|^2\right) + (ma)x \qquad (7)$$

Figs. 11 and 12 show the evolution of the BEC and optical fields for the cases of red and blue detuning respectively. It can be seen that the BEC now accelerates uniformly, and as for the case of uniform motion, the optical field follows this motion with the BEC density coinciding with an optical intensity maximum or minimum for red and blue detuning respectively.

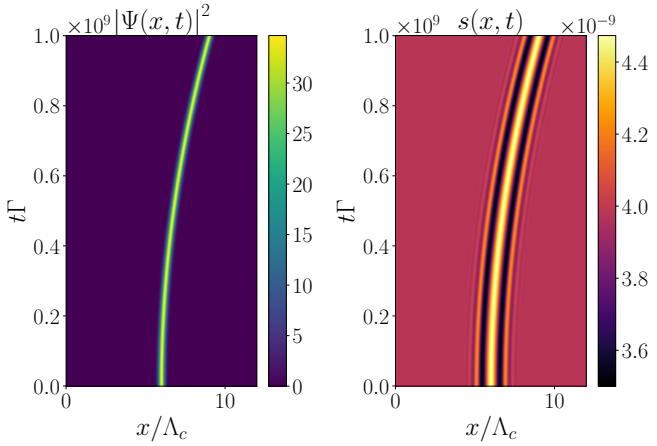

FIG. 11. Uniformly accelerating droplet for red-detuning ($\Delta < 0$). Parameters used are identical those of Fig. 3 with the addition of $a = -4.0 \times 10^{-9}(\hbar q_c \Gamma/12m)$.

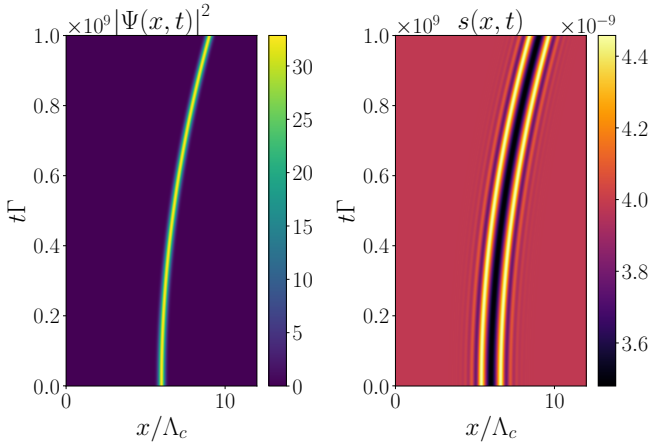

FIG. 12. Uniformly accelerating droplet for blue-detuning ($\Delta > 0$). Parameters used are identical those of Fig. 4 with the addition of $a = -4.0 \times 10^{-9}(\hbar q_c \Gamma/12m)$.

Figs. 9 and 10 for uniform motion and Figs. 11 and 12 for uniform acceleration show that in both cases, it is possible to infer the distribution of BEC density continuously via observation of the optical intensity distribution.

It should be noted that although only the motion of single droplet structures has been presented here, the stable multi-peak droplet structures display similar behaviour under motion, maintaining their structure as they propagate and providing a consistent optical intensity profile dependant on detuning.

C. Controlling Droplet Motion Using Mirror Tilt

In the previous section we demonstrated how imposing a uniform velocity or acceleration on the BEC could produce an optomechanical droplet with a BEC density distribution and optical field distribution which moved with uniform velocity or uniform acceleration respectively. We now investigate what happens when the mirror in the SFM configuration is not perfectly aligned, so that the normal to the mirror and the pump propagation direction are misaligned by a small angle, α. This mirror misalignment or tilt is shown schematically in Fig. 13.

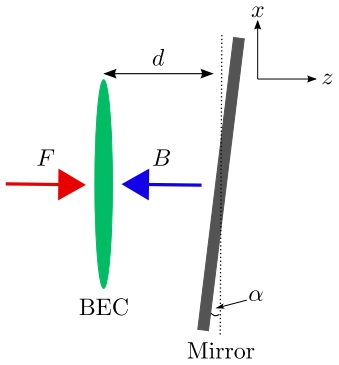

FIG. 13. Schematic diagram of the single mirror feedback (SFM) configuration with a mirror misalignment/tilt, labelled α.

In order to simulate the effect of this mirror tilt, we follow the method used in [38], where before calculation of the backward field, B, using Eq. 4, the forward field is shifted by an amount $\Delta x = 2d\tan(\alpha)$. The effect of a mirror tilt can also be understood as creating a phase gradient in the reflected light. An example of evolution of an initially stationary droplet ($v_0 = a = 0$) with $\Delta x > 0$ is shown in Fig. 14. It can be seen that the effect of the mirror tilt is to produce a constant acceleration on the droplet.

Fig. 15 shows the dependence of the droplet acceleration on the mirror tilt induced shift, Δx. It can be

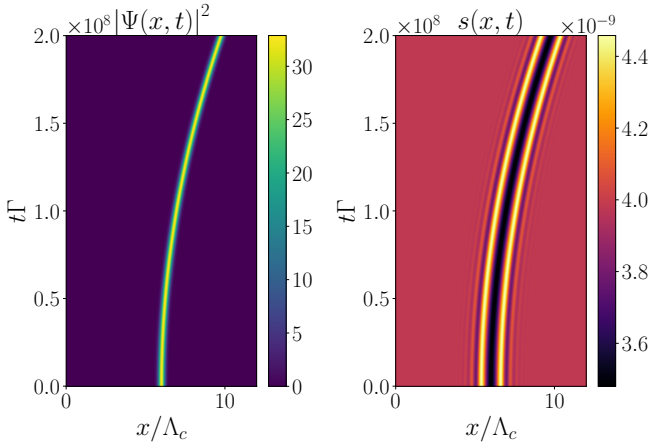

FIG. 14. Evolution of BEC density and optical field intensity when a mirror tilt is present. Parameters used are: $p_0 = 1.9 \times 10^{-9}$, $\Delta = 800$, $R = 0.99$, $\omega_r/\Gamma = 5.69 \times 10^{-8}$, $b_0 = 20$ and $\Delta x/\Lambda_c = 1.465 \times 10^{-3}$.

seen that for the smallest mirror tilts, the acceleration produced is approximately proportional to Δx and consequently α. However, as the mirror tilt is increased, there is a region where the acceleration produced changes direction. Similar behaviour was observed for dissipative solitons [34] however a significant difference between the behaviour shown here and that in [34] is that here the droplets exhibit Newtonian dynamics whereas in [34] the solitons exhibited Aristotelian dynamics.

Dynamics of dissipative solitons in phase gradients are known from many such dissipative systems. However, the dynamics are Aristotelian in nature as overdamped motion exhibits a constant velocity in the presence of a constant gradient [34, 39, 40]. The acceleration consistent with Newtonian motion in the BEC model considered here is a novel feature of conservative optomechanical systems, in comparison to dissipative solitons relying on internal degrees of freedom [34, 39, 40] or optomechanical structures and solitons in the presence of velocity damping [41, 42].

Laser solitons in which the medium dynamics is infinitely fast should also exhibit Newtonian dynamics [9, 43] but we are not aware of any experimental observation, as typical lasers do not operate in this regime. In contrast, observation in a BEC system, similar to that discussed here, would appear to be very feasible.

In addition to inducing acceleration of the droplet, the application of a finite mirror tilt also decreases the long term stability of the droplet, with stability of the structures preserved for only very small misalignments.

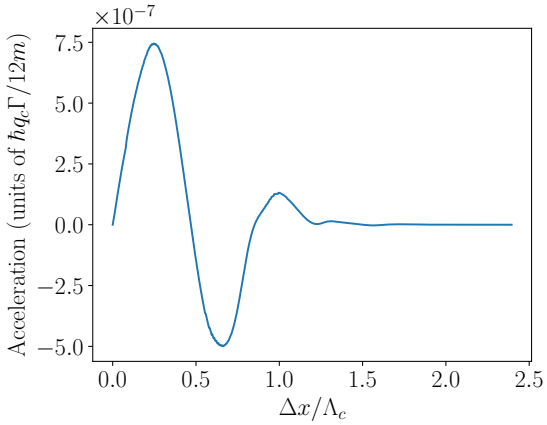

FIG. 15. Dependence of droplet acceleration, a_d, on mirror tilt-induced shift, $\Delta x/\Lambda_c$. Parameters used are: $p_0 = 1.9 \times 10^{-9}$, $\Delta = 200$, $R = 0.99$, $\omega_r/\Gamma = 1.01 \times 10^{-7}$ and $b_0 = 20$.

IV. CONCLUSIONS

We have investigated the dynamical behaviour of optomechanical droplets, self-bound structures which arise due to the interaction between light and a BEC in the presence of a feedback mirror, using a 1D model. We have shown the existence of multi-peak droplet profiles from optical interactions alone, when atomic collisions are negligible. We have also shown that by inducing BEC motion with constant velocity and constant acceleration, the optomechanical droplets remain stable and also move with the same velocity and acceleration respectively, with the BEC density maximum being tracked by the optical field pattern in each case. As the pump is far-detuned from resonance, absorption and therefore heating of the BEC due to scattering of pump photons is minimised. Consequently these results may offer new possibilities for methods allowing continuous measurement of BEC dynamics. Finally, we demonstrated that by introducing a mirror misalignment/tilt it was possible to induce a constant droplet acceleration. This may offer new opportunities for optical control and transport of coherent matter via phase gradients rather than amplitude gradients. Possibilities for future development of the results presented here include investigation of the dynamics of droplets in 2D and the inclusion of atomic collisions i.e. non-zero scattering length in the BEC, as [30] showed that the inclusion of non-zero scattering length leads to other more complex structures e.g. droplet chains and lattices, in addition to the single and novel multi-peak droplets considered here.

[1] M. C. Cross and P. C. Hohenberg, Pattern formation outside of equilibrium, Reviews of modern physics **65**, 851 (1993).

[2] G. Grynberg, E. Le Bihan, P. Verkerk, P. Simoneau, J. R. Leite, D. Bloch, S. Le Boiteux, and M. Ducloy, Observation of instabilities due to mirrorless four-wave mixing oscillation in sodium, Optics communications **67**, 363 (1988).

[3] G. Lippi, T. Ackemann, L. Hoffer, and W. Lange, Transverse structures in a sodium-filled fabry-pérot resonator—i. experimental results: Symmetries and the role of the incoupling conditions, Chaos, Solitons & Fractals **4**, 1409 (1994).

[4] G. Lippi, T. Ackemann, L. Hoffer, and W. Lange, Transverse structures in a sodium-filled fabry-pérot resonator—ii. interpretation of experimental results, Chaos, Solitons & Fractals **4**, 1433 (1994).

[5] G. Giusfredi, J. Valley, R. Pon, G. Khitrova, and H. Gibbs, Optical instabilities in sodium vapor, JOSA B **5**, 1181 (1988).

[6] W. Firth, Spatial instabilities in a kerr medium with single feedback mirror, Journal of Modern Optics **37**, 151 (1990).

[7] F. T. Arecchi, S. Boccaletti, and P. L. Ramazza, Pattern formation and competition in nonlinear optics, Phys. Rep. **318**, 1 (1999).

[8] L. A. Lugiato, Transverse nonlinear optics: Introduction and review (Editorial to special issue: Nonlinear optical structures, patterns, chaos), Chaos, Solitons & Fractals **4**, 1251 (1994).

[9] N. N. Rosanov, Transverse patterns in wide-aperture nonlinear optical systems, Progress in Optics **XXXV**, 1 (1996).

[10] S. Barbay, R. Kuszelewicz, and J. R. Tredicce, Cavity Solitons in VCSEL Devices, Adv. Opt. Tech. **2011**, 628761 (2011).

[11] G. Grynberg, A. Maître, and A. Petrossian, Flowerlike patterns generated by a laser beam transmitted through a rubidium cell with a single feedback mirror, Phys. Rev. Lett. **72**, 2379 (1994).

[12] T. Ackemann and W. Lange, Non- and nearly hexagonal patterns in sodium vapor generated by single-mirror feedback, Phys. Rev. A **50**, R4468 (1994).

[13] T. Ackemann and W. Lange, Optical pattern formation in alkali metal vapors: Mechanisms, phenomena and use, Appl. Phys. B **72**, 21 (2001).

[14] D. Kruse, C. von Cube, C. Zimmermann, and P. W. Courteille, Observation of lasing mediated by collective atomic recoil, Physical review letters **91**, 183601 (2003).

[15] H. Ritsch, P. Domokos, F. Brennecke, and T. Esslinger, Cold atoms in cavity-generated dynamical optical potentials, Reviews of Modern Physics **85**, 553 (2013).

[16] F. Mivehvar, F. Piazza, T. Donner, and H. Ritsch, Cavity qed with quantum gases: new paradigms in many-body physics, Advances in Physics **70**, 1 (2021), https://doi.org/10.1080/00018732.2021.1969727.

[17] A. J. Kollar, A. T. Papageorge, V. D. Vaidya, Y. Guo, J. Keeling, and B. L. Lev, Supermode-density-wave-polariton condensation with a Bose–Einstein condensate in a multimode cavity, Nat. Commun. **8**, 14386 (2017).

[18] R. M. Kroeze, Y. Guo, V. D. Vaidya, J. Keeling, and B. L. Lev, Spinor self-ordering of a quantum gas in a cavity, Physical review letters **121**, 163601 (2018).

[19] Y. Guo, R. M. Kroeze, B. P. Marsh, S. Gopalakrishnan, J. Keeling, and B. L. Lev, An optical lattice with sound, Nature **599**, 211 (2021).

[20] G. Robb, N. Piovella, A. Ferraro, R. Bonifacio, P. W. Courteille, and C. Zimmermann, Collective atomic recoil lasing including friction and diffusion effects, Physical Review A **69**, 041403 (2004).

[21] K. Baumann, C. Guerlin, F. Brennecke, and T. Esslinger, Dicke quantum phase transition with a superfluid gas in an optical cavity, nature **464**, 1301 (2010).

[22] R. Mottl, F. Brennecke, K. Baumann, R. Landig, T. Donner, and T. Esslinger, Roton-type mode softening in a quantum gas with cavity-mediated long-range interactions, Science **336**, 1570 (2012).

[23] S. Schuster, P. Wolf, S. Ostermann, S. Slama, and C. Zimmermann, Supersolid properties of a bose-einstein condensate in a ring resonator, Physical review letters **124**, 143602 (2020).

[24] J. Léonard, A. Morales, P. Zupancic, T. Esslinger, and T. Donner, Supersolid formation in a quantum gas breaking a continuous translational symmetry, Nature **543**, 87 (2017).

[25] J. A. Greenberg, B. L. Schmittberger, and D. Gauthier, Bunching-induced optical nonlinearity and instability in cold atoms, Opt. Exp. **19**, 22535 (2011).

[26] B. L. Schmittberger and D. J. Gauthier, Spontaneous emergence of free-space optical and atomic patterns, New J. Phys. **18**, 10302 (2016).

[27] G. Labeyrie, E. Tesio, P. M. Gomes, G.-L. Oppo, W. J. Firth, G. R. Robb, A. S. Arnold, R. Kaiser, and T. Ackemann, Optomechanical self-structuring in a cold atomic gas, Nature Photonics **8**, 321 (2014).

[28] E. Tesio, *Theory of self-organisation in cold atoms*, Ph.D. thesis, University of Strathclyde (2014).

[29] G. Robb, E. Tesio, G.-L. Oppo, W. Firth, T. Ackemann, and R. Bonifacio, Quantum threshold for optomechanical self-structuring in a bose-einstein condensate, Physical review letters **114**, 173903 (2015).

[30] Y.-C. Zhang, V. Walther, and T. Pohl, Long-range interactions and symmetry breaking in quantum gases through optical feedback, Physical review letters **121**, 073604 (2018).

[31] Y.-C. Zhang, V. Walther, and T. Pohl, Self-bound droplet clusters in laser-driven bose-einstein condensates, Physical Review A **103**, 023308 (2021).

[32] J. Qin and L. Zhou, Self-trapped atomic matter wave in a ring cavity, Physical Review A **102**, 063309 (2020).

[33] M. Edmonds, T. Bland, and N. Parker, Quantum droplets of quasi-one-dimensional dipolar bose–einstein condensates, Journal of Physics Communications **4**, 125008 (2020).

[34] T. Ackemann, W. Firth, and G.-L. Oppo, Fundamentals and applications of spatial dissipative solitons in photonic devices, Advances in atomic, molecular, and optical physics **57**, 323 (2009).

[35] T. Ackemann, G. Labeyrie, G. Baio, I. Krešić, J. Walker, A. Costa Boquete, P. Griffin, W. Firth, R. Kaiser, G.-L. Oppo, and G. Robb, Self-organization in cold atoms

mediated by diffractive coupling, Atoms **9**, 35 (2021).
[36] G. Robb, J. Walker, G.-L. Oppo, and T. Ackemann, in preparation, (2021).
[37] R. Plestid and D. O'Dell, Balancing long-range interactions and quantum pressure: Solitons in the hamiltonian mean-field model, Physical Review E **100**, 022216 (2019).
[38] B. Schäpers, T. Ackemann, J. Seipenbusch, and W. Lange, Nonequilateral drifting hexagons in a strongly misaligned single-mirror system, Journal of Optics B: Quantum and Semiclassical Optics **1**, 58 (1999).
[39] W. J. Firth and A. J. Scroggie, Optical bullet holes: robust controllable localized states of a nonlinear cavity, Phys. Rev. Lett. **76**, 1623 (1996).
[40] T. Maggipinto, M. Brambilla, G. K. Harkness, and W. J. Firth, Cavity solitons in semiconductor microresonators: Existence, stability, and dynamical properties, Phys. Rev. E **62**, 8726 (2000).
[41] G. Labeyrie, E. Tesio, P. Gomes, G.-L. Oppo, W. Firth, G. Robb, A. Arnold, R. Kaiser, and T. Ackemann, Nonlinear optomechanical patterns and dissipative solitons, in *Nonlinear Photonics* (Optical Society of America, 2014) pp. NTh1A–4.
[42] G. Baio, G. R. Robb, A. M. Yao, G.-L. Oppo, and T. Ackemann, Multiple self-organized phases and spatial solitons in cold atoms mediated by optical feedback, Physical Review Letters **126**, 203201 (2021).
[43] S. V. Fedorov, A. G. Vladimirov, G. V. Khodova, and N. N. Rosanov, Effect of frequency detunings and finite relaxation rates on laser localized structures, Phys. Rev. E **61**, 5814 (2000).